Chapter 8 Vanadium Oxide Films

8.1. Introduction

Vanadium exists in a number of oxide forms, the di-, sesqui- and pentoxides (VO_2, V_2O_3 and V_2O_5). They have been processed in thin film form and applied as optical and electrical devices. Especially vanadium oxide (V_2O_5), as a wide band gap and n-type semiconductor material, was widely investigated because of its interesting electrochemical performance [1-2], is integration in lithium secondary batteries [3], and its thermochromic [4-6] and electrochromic properties [7-8]. In addition, vanadium oxides are added to SnO_2 to increase the sensitivity and selectivity of the sensors to aromatic hydrocarbons [9-10]. Ultra-thin layers of vanadium oxides can be used as model systems of gas sensing surfaces to obtain detailed information at atomic level concerning the structure and composition of the surface and interface. The large lithium insertion capability, theoretically up to two equivalent of lithium per vanadium, makes it attractive for use as a cathode in high-capacity lithium batteries. V_2O_5 films have been successfully employed in electrochromic devices (ECDs) as counter electrodes (or passive lithium reservoirs). The V_2O_5 ion storage can be a Li^+ doped thin film prepared by an electrochemical or vacuum deposition method. It leads to an increase of the coloration efficiency of ECDs. They have high ion-storage capacity of 20~30 mC/cm^2 in the 4.8 to 1.8 V potential range, long term electrochemical stability (few thousand cycles) and moderate optical transmittance modulation [$\Delta T_{vis} = T_{vis}$(coloured) – T_{vis} (bleached)] when charged/discharged in the safe potential range.

Up to now Moshfegh *et al.* [11] reported on the stoichiometry of V_2O_5 films formed by oxidising a vanadium substrate at different partial pressures. Benmoussa *et al.* and Kusano *et al.* reported on the stoichiometry and deposition conditions of the films prepared by rf [12] and dc sputtering [13].

Films of mixed vanadium-molybdenum (or titanium) oxides [14-15] and other mixed transition metal oxides [15-18] have been recognised as promising materials for counter-electrodes in ECDs. The cycling data showed that vanadium mixed oxides exhibit a better reversibility than V_2O_5 alone. Among these films, vanadium-molybdenum films

seem to have approximately the same electrochemical behaviour as that of vanadium-titanium oxides and exhibit better performances.

Molybdenum trioxide (MoO_3) possesses structural, electrical and optical properties similar to those of V_2O_5. It is an important partial oxidation catalyst that is also of interest in gas sensing applications[19]. Oxygen deficient MoO_3 exhibits photochromic and electrochromic properties. The ability of MoO_3 films to reversibly exchange lithium ions with an electrolyte and electrons with an external circuit was explored in ECDs [7]. The deposited films are slightly blue (or transparent) and show a deep blue colour after Li^+ has been inserted. The physical and chemical properties of bulk V_2O_5-MoO_3 [20] and $(V_2O_5)_{1-x}$ - $(MoO_3)_x$ in the composition range $0<x<1$ have been reported by few workers [16, 21].

In addition to electrochromic properties both vanadium oxide and molybdenum trioxide can present photochromic (PC) and thermochromic (TC) properties in which the formation of colour centres by light irradiation and temperature effect happen [22]. TC materials exhibit reversible optical and electrical properties with changing temperature. That is, via an abrupt crystallographic phase transition at a critical temperature (T_c), they change optically from a NIR transmitting to NIR reflecting material and electrically from a semiconductor to a metallic material. Generally vanadium dioxide is one of the most interesting materials for TC windows [23-24]. It has been used in advanced windows for the automatic control of energy throughputs[25] (solar or high temperature radiate energy). Jin *et al.* [24] have studied the relationship between T_c and W doping for sputter-deposited $V_{1-x}W_xO_2$ films. $V_{1-x}Mo_xO_2$ film was searched by them for TC applications too [4]. In their study, replacing V^{4+} with W^{6+} introduces extra electrons into the crystal lattice of VO_2, resulting in the reduction of T_c via a charge transfer mechanism. Doping with Mo could result in a same conclusion. Similarly, V_2O_5 doping with Mo should become another candidate for TC applications or TC windows. Although a number of studies were performed on W or Mo doped VO_2 films, the TC film study on V_2O_5 or Mo-doped V_2O_5 has been up to now extremely limited for TC applications.

Here we investigate the effect of the substrate temperature during deposition on the microstructure and properties of the V_2O_5 and Mo-doped V_2O_5 films. The use of UV-visible-NIR spectra, XPS, XRD and IR spectroscopies have allowed us to obtain important information from the scientific point of view, as well as applications. The

thermochromic and thermotropic properties of V_2O_5 and MoO_3 doped V_2O_5 films will be discussed in detail.

8.2. V_2O_5 and MoO_3 Structure

Vanadia, chemically V_2O_5, possesses a layer structure built up of VO_5 square pyramids sharing edges and corners[26]. The VO_5 pyramids sharing edges always have opposite orientations to maximize distances between the vanadium cations. At the same time taking into account distant oxygen atoms (2.793 Å) from the adjacent layer, one can consider coordination polyhedra of vanadium atoms as distorted octahedrons. V_2O_5 has an orthorhombic lattice structure with bulk parameters a_0=11.519 Å, b_0=4.373 Å and c_0=3.564 Å. The extended space lattice consists of alternating layers of vanadium plus oxygen atoms and oxygen atoms (vanadyl oxygen) alone oriented parallel to the b axis or <010> crystallographic direction as shown in Fig. 8-2-1[27].

For molybdenum trioxide, the polymorphs are constructed from distorted MoO_6-octahedra[28]. The MoO_3 has a layered structure consisting of double layers of MoO_6-octahedra held together by covalent forces.

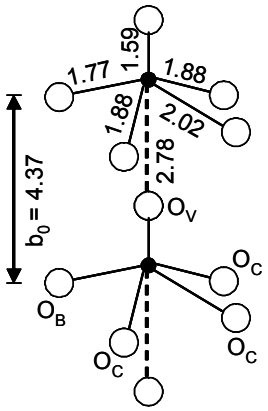


Fig. 8-2-1. The effective fivefold coordination of vanadium with oxygen in the perfect vanadia lattice. Dark circles represent vanadium atoms; white circles represent oxygen atoms: Ov, vanadyl oxygen; Oc, chain oxygen; O_B, bridge oxygen. Bond lengths are shown in angstrom (Å) unit.

8.3. UV-Vis-NIR Spectra of the Films

Some good transmittance spectra of the films are shown in Fig. 8-3-1~8-3-4. The effect of substrate temperature (T_s) during film deposition is shown in Fig. 8-3-1. The films were grown with 15% P_{O2} in 1.2 Pa P_T (total pressure of sputtering) for 20

minutes. As T_s increases from RT to 400 ^{0}C, the average transmittance of the film decreases, the film thickness increases and the colour of the film changes from light yellow to yellow at the higher T_s.

The effect of Mo-doping percentage on the transmittance of the films is shown in Fig. 8-3-2. The films were grown with 20% P_{O2} and using different deposition times. As the Mo doping ratio increases from 0 to 18.9%, the transmittance intensity of the films remains approximately similar. The absorption edge (~450 nm) of transmittance of the films shifts to short wavelength direction as the ratio of doped Mo increases and that means the transmittance spectra widens.

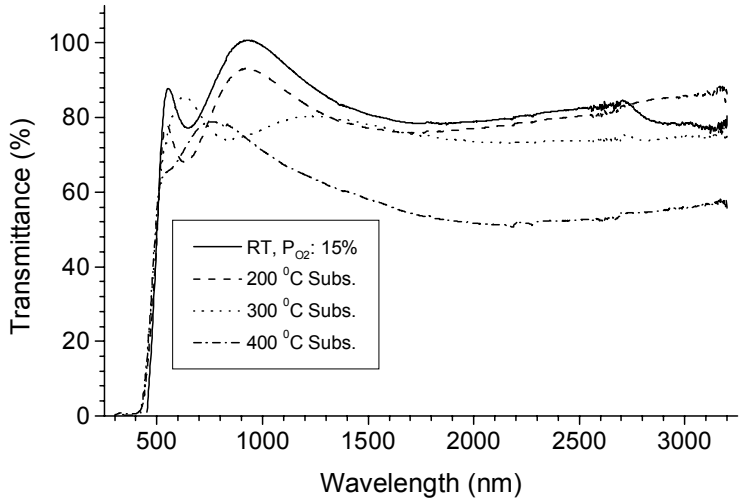


Fig. 8-3-1. Transmittance of the samples grown with 15% P_{O2}, room temperature and different substrate temperatures.

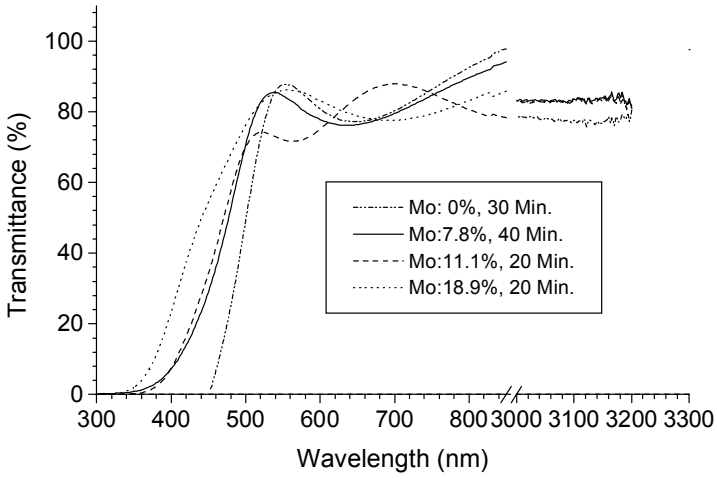


Fig. 8-3-2. Transmittances of samples grown with 20% $P_{O2,}$ different Mo-doped ratio (area ratio of the vanadium and molybdenum on the erosion surface of the target) and different deposition time.

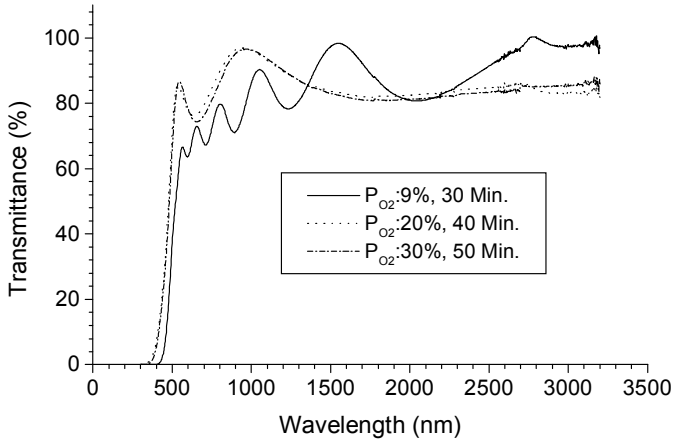


Fig. 8-3-3. Transmittance of 7.8% Mo doped films grown with different P_{O2} and different deposition times.

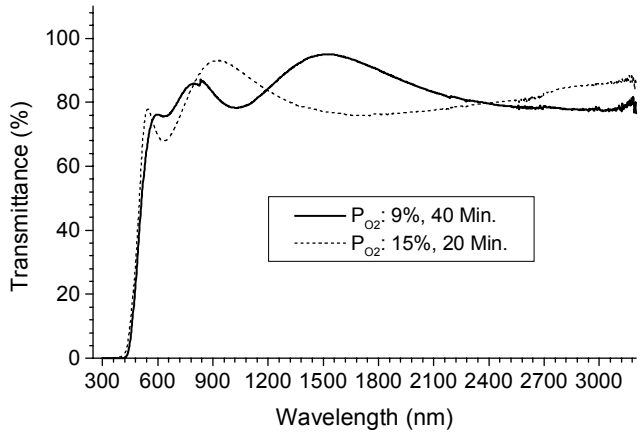


Fig. 8-3-4. Transmittance of films grown at 200 ^{0}C substrate temperature in 9% and 15% P_{O2}.

Fig. 8-3-3 shows the effect on P_{O2} of the films. The films are grown at different P_{O2} and different times by using the vanadium target with 7.8% Mo doping (area ratio of the vanadium and molybdenum on the erosion surface of the target). As the P_{O2} increases from 9% to 30%, the transmittance of the films has a tendency to increase, for wavelengths less than 1300 nm.

Fig. 8-3-4 illustrates the effect on P_{O2} of film deposition, in which the film was grown at 200 ^{0}C T_s. The 9% P_{O2} film has higher transmittance in the most wavelength range. The transmittances of all V_2O_5 samples are over 68% in visible region.

8.4. IR Vibration Characteristics of the Films

According to the results of the theoretical analysis, 21 modes of vibration are possible in the Raman and 15 modes in the IR spectrum of the V_2O_5. IR spectra of V_2O_5 and V_2O_5-MoO_3 films (Fig. 8-4-1 and Fig. 8-4-4) were recorded in the wavenumber range

400-4000 cm^{-1}. The band appearing at 975 and 1020 cm^{-1} correspond to the V (vanadium)-O_v (vanadyl oxygen) stretching mode. The band between 700 and 900 cm^{-1} is assigned to the anti-symmetric stretching vibration of the V-O_b-V group (O_b: bridge oxygen). The group of bands present at <600 cm^{-1} wavenumber correspond to the edge-shearing 3V-Oc stretching and the bridging V-O_b-V deformations [29, 30]. The shift of the strong band between 1140 cm^{-1} and 1220 cm^{-1}, which is assigned to δ(w-o) in the M-OH…H_2O group, was observed as the plane deformational (bending) M-O mode. Detailed assignment of these modes determined from the NGIA (near grazing incidence angle) IR reflection-absorbance spectra are given in Table 8-4-1 and discussed in the following paragraphs.

The effect of the annealing on the behavior of the films grown with 20% P_{O2} and 9% P_{O2}, is shown in Fig. 8-4-1 and Fig. 8-4-2 respectively. It is seen that as the temperature increases from RT to 400 ^{0}C, the peak at 970 cm^{-1}, the shoulder peak at 1020 cm^{-1} and the band at 1220 cm^{-1} (or 1182 cm^{-1}) of the films increases and the peaks at 517 and 418 cm^{-1} decrease. The colour of the film changed from light yellow to dark yellow at higher annealing temperature (T_a). The M-O band of M-OH…H_2O group in V_2O_5 film increases and shifts to lower wavenumbers after annealing. This is due to the removing of the adsorbed water on the surface of the film. Fig. 8-4-3 and Fig. 8-4-4 confirm these results. The fact that nearly no change of the intensity and position of the M-O band shows that it is a characteristic of the inter-structure (M-O) of the film.

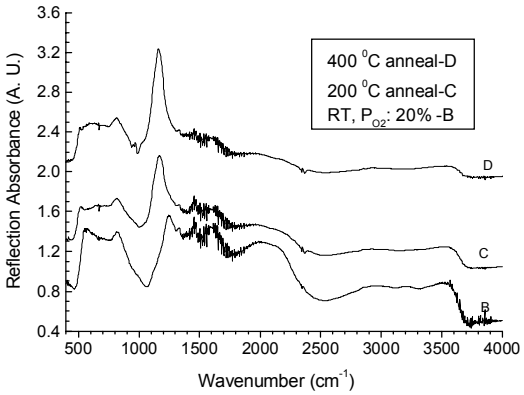


Fig. 8-4-1. IR spectra of the V_2O_5 samples grown with 20% P_{O2}, at room temperature, plus 200 ^{0}C and 400 ^{0}C annealing respectively.

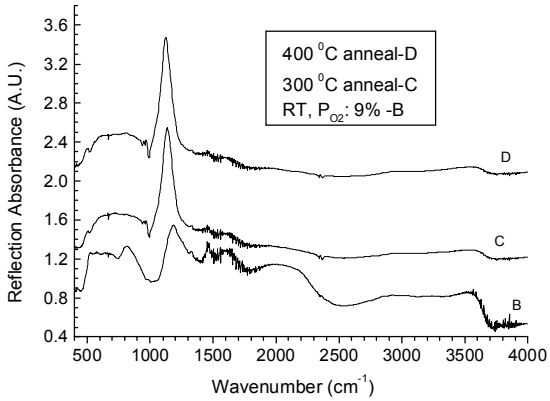


Fig. 8-4-2. IR spectra of the V_2O_5 samples grown with 9% P_{O2}, at room temperature, plus 300 ^{0}C and 400 ^{0}C annealing respectively.

The effect of the deposition P_{O2} of the film that was grown at 200 ^{0}C substrate temperatures (T_s) in 15% P_{O2} and 9% P_{O2} is shown in Fig. 8-4-3. It is seen that the

absorbance peaks 970 and 1020 cm^{-1} of the films become stronger after depositing at 200 ^0C T_s. The thickness increased a little and the color of the film changed from light yellow to yellow at the higher T_s.

On the basis of the structural properties of MoO_3- formed by MoO_6- octahedral, the stretching and bending vibrational modes occur mainly in the range 1050-500 cm^{-1}. The stretching mode of the (O-Mo) terminal at about 991 cm^{-1} is a unique characteristic of the layered α-MoO_3 structure. The IR stretching modes due to the alternating bond lengths are at 478, 612 and 870 cm^{-1} [31].

The effect of Mo-doping on behavior of the film is shown in Fig. 8-4-4. The films were deposited with 20% P_{O2} and 30% P_{O2}. It is seen that as the ratio of Mo doping increases from 0 to 18.9%, the absorbance peak of the 20% P_{O2} films has no clear change. With the same Mo doping ratio (18.9%), the peak 816 cm^{-1} of the film (sample E) with 30% P_{O2} shifts to lower wavenumbers comparing with sample D with 20% P_{O2}.

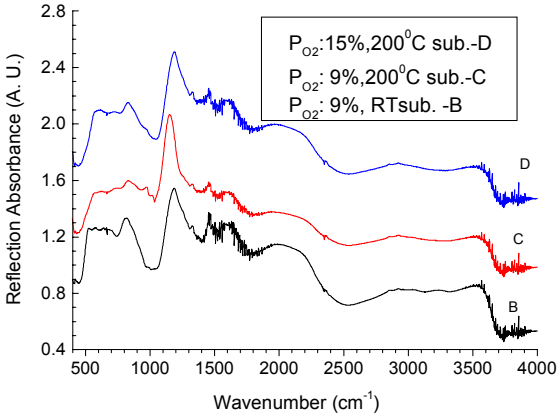


Fig. 8-4-3. IR spectra of the V_2O_5 films grown at room temperature and 200 ^0C substrate temperature with 9% and 15% P_{O2} respectively.

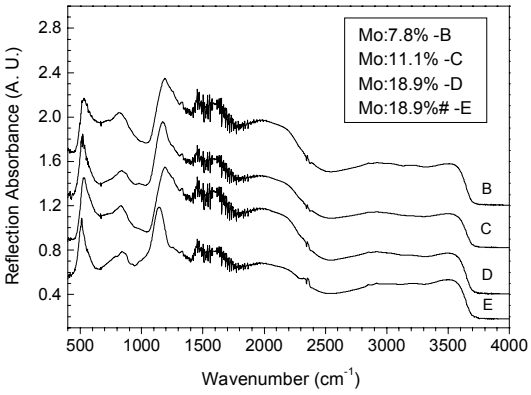


Fig. 8-4-4. IR spectra of the V_2O_5 films grown with different Mo doping ratios and 20% P_{O2}; # Curve E is the film grown with 30% P_{O2}.

The IR results show that the deposited film is V_2O_5 and VO_2, because the shoulder peaks at 508 cm^{-1} and 714 cm^{-1} of VO_2 does not appear in those IR spectra too. The XRD analysis in Section 8.8 also confirms IR results. In Fig. 8-4-4 there is clearly an increase of the 535 cm^{-1} peak of MoO_3, as the Mo-doping ratio is increased. All these are confirmed by the XPS study (Section 8.7). The IR spectra of V_2O_5–MoO_3 films show poorly resolved broad bands and they are found to be more or less similar to that of V_2O_5 in our experiments, for less than 20% Mo-doping ratio. This indicates that the structure of V_2O_5 is not deeply modified upon the incorporation of these quantities of MoO_3.

Table 8-4-1. IR vibrational modes of the films (Wavenumbers: cm^{-1})

Exp.	Assi.	V_2O_5 ref.	VO_2 ref.	V_2O_3 ref.
418w	$\nu(3V\text{-}O_C)$	412 [32]		
		490 [33]		
509m	$\nu(3V\text{-}O_C)$	507 [34]	508sh [35]	
517m		512 [35]		520sh [35]
717m	$\nu(V\text{-}O_b\text{-}V)$	767 [34]	714sh [35]	
		784 [33]		
804m	$\nu(3V\text{-}O_C)$	842 [34]		
816m		828 [35]		
970m		975 [32]		980 [35]
MoO_3 film				
478-612	O-Mo Ter	478 [33]		
		535 [33]		
		612 [33]		
		870 [31]		

Exp.: experiment, ref. reference, Assi.: assignment, m: medium, sh: shoulder peak, w: weak, Ter.: terminal.

8.5. Thermochromic Properties of the Films

The IR transmittance spectra of the films are shown in curves from Fig. 8-5-1 to Fig. 8-5-4, in the 3000~4000 cm^{-1} range (3.3~2.5 μm), before and after these samples are put into 200 ^{0}C temperature environment. The films exhibit clear changes in transmittance, especially in the range 3600-4000cm^{-1}. The variation of the transmittance arises due to the films change from a semiconductor phase to a metallic phase [4]. The data is summarized in the table 8-5-1.

Fig. 8-5-1 shows that after applying higher T ($>T_c$) to the as-deposited films (sample V1; V2; V3) deposited with different P_{O2}, at room temperature and 400^{0}C substrate temperature, the transmittance changes reaching a value up to 30%. The films deposited at 400 ^{0}C heated substrate show little variation.

Fig. 8-5-2 shows that the 200 ^{0}C annealed films (sample V1a; V3a; V4a) have strong transmittance variance, after applying higher T ($>T_c$) to these samples which were deposited with different P_{O2} and were different annealing temperatures treated at different annealing temperatures. The maximum variation of the transmittance reaches 39 % between sample D and E at 4000 cm^{-1} wavenumber.

Table 8-5-1. Deposition onditions, parameters and a thermochromic properties of V_2O_5 films and Mo doped V_2O_5 films.

Sample	P_{O2} (%)	Ratio of Mo (%)	T_s (^{0}C)	T_a (^{0}C)	IR $_{at\ RT}$ T_{ts}(%)	IR $_{at\ 200\ ^0C}$ T_{ts}(%)	Δ IR (%)
V1	9	-	RT	-	79.0	49.0	30.0
V2	15	-	400	-	26.0	22.5	3.5
V3	20	-	RT	-	83.0	66.0	17.0
V1a	9	-	RT	400	27.5	16.0	11.5
V3a	20	-	RT	400	32.5	15.0	17.5
V4a	20	-	RT	200	53.0	14.0	39.0
VM1	9	7.8	RT	-	94.0	58.0	36.0
VM2	20	7.8	RT	-	86.5	42.5	44.0
VM3	30	7.8	RT	-	87.5	45.0	42.5
VM4	20	11.1	RT	-	82.5	43.0	39.5
VM5	20	18.9	RT	-	86.5	37.5	49.0

ΔIR: transmittance different at the 4000 cm^{-1} (2.5 μm) before and after the sample is put into 200 ^{0}C temperature environment, ΔIR= IR $_{at\ 200\ ^0C}$ - IR $_{at\ RT.}$

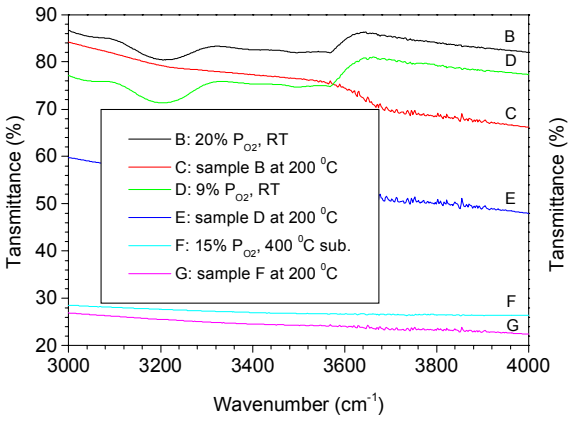


Fig. 8-5-1. IR spectra of films (sample V1=D; V2=F; V3=B) deposited with different P_{O2} before and after putting them into 200 ^{0}C environment.

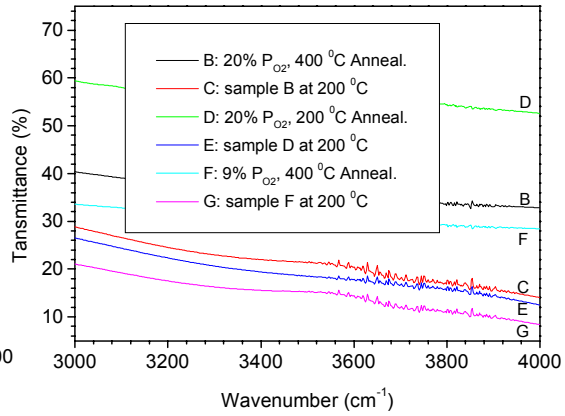


Fig. 8-5-2. IR spectra of the annealed films (sample V1a=F; V3a=B; V4a=D) before and after putting them into 200 ^{0}C environment.

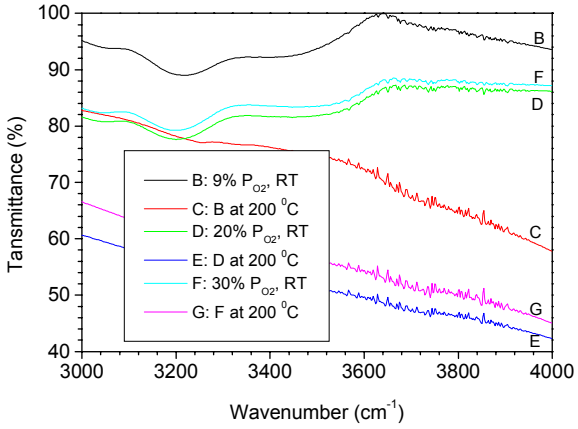


Fig. 8-5-3. IR spectra of the 7.8% doped Mo films (sample VM1=B; VM2=D; VM3=F) deposited with different P_{O2} before and after applying 200 ^{0}C to the samples.

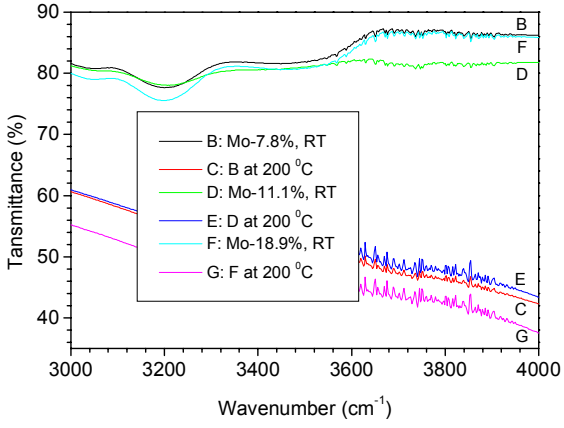


Fig. 8-5-4. IR spectra of the 20% P_{O2} films (sample VM2=B; VM4=D; VM5=F) deposited with the different ratios of Mo doping before and after applying 200 ^{0}C to the samples.

Fig. 8-5-3 shows IR spectra of the 7.8% doped Mo films (sample VM1; VM2; VM3) deposited with different P_{O2} before and after applying 200 ^{0}C to the samples. After applying temperature of 200 ^{0}C to the 7.8% Mo doped samples, the variation of transmittance for all samples is from 36% to 44% at 4000 cm^{-1} wavenumber. There is tendency of bigger variation of transmittance when the P_{O2} of the film is larger, after applying temperature of 200 ^{0}C to the samples

Fig. 8-5-4 shows IR spectra of the 20% P_{O2} films (sample VM2; VM4; VM5) deposited with the different ratios of Mo doping before and after applying 200 ^{0}C to the samples. There is tendency of bigger variation of transmittance when the Mo doping ratio of the film is larger, after applying temperature of 200 ^{0}C to the samples. The maxmium variation of transmittance among samples reaches 49% at 4000 cm^{-1}. All these properties of the films indicate that V_2O_5 films have good thermochromic behaviors in the range 3600-4000 cm^{-1}. They are ideal TC materials.

8.6. Thermo-resistance (Thermotropic) Property of the Films

Thermotropic (TT) switching occurs as an electronic transformation in specific transition metal oxides and related compounds, when a "critical" temperature is exceeded in the material. Some of these compounds are Fe_3O_4, $FeSi_2$, NbO_2, NiS, Ti_2O_3, VO_2, and V_2O_3 [36]. These are known as the Mott transition compounds [37]. Such materials can be also used to control transmittance and infrared emissivity of a glazing.

Table 8-6-1. Deposition conditions, the parameters and thermo-resistance of V_2O_5 films and Mo doped V_2O_5 films.

Sample	P_{O2} (%)	Ratio of Mo (%)	T_s (^{0}C)	T_a (^{0}C)	$\Delta R_{2p\ max}/T$ (Ω / ^{0}C)
V1a	9	-	RT	400	0.8
V6	9	-	RT	300	2.3
V3a	20	-	RT	400	40.0
V4a	20	-	RT	200	52.0
V2	15	-	400	-	3.0
V7	15	-	200	-	260.0
V8	9	-	200	-	160.0
VM2a2	20	7.8	RT	200	560.0
VM2a4	20	7.8	RT	400	1200.0

$\Delta R_{2p\ max}/T$: The maximum change of the R_{2p}/T rate (ohm per centigrade degree) in case of changing of the environment temperature.

The influence of the temperature (T) on the electrical resistance (R) or electrical resistivity was investigated. Resistance between two points (R_{2P}) 1 cm apart, on the surface of the film, was measured. The curves of T- R_{2P} were recorded by increasing and decreasing the applied temperature to the samples, and are shown in Fig. 8-6-1 to Fig. 8-6-4. All the films except the ones grown at RT exhibit clear changes in resistance in the RT-350 ^{0}C range. The films grown at RT had no resistivity variance in the range RT-100 ^{0}C. The data is summarized in the table 8-6-1.

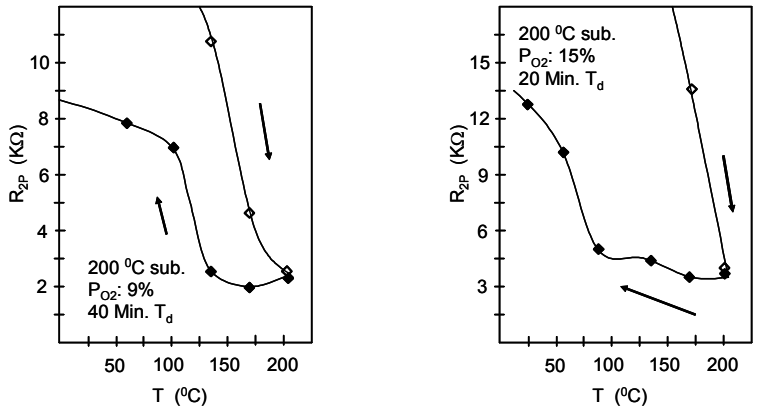


Fig. 8-6-1. Thermo-resistance curves of the films (sample V8 and V7) grown at 200 ^{0}C substrate temperature with 9% and 15% P_{O2} respectively.

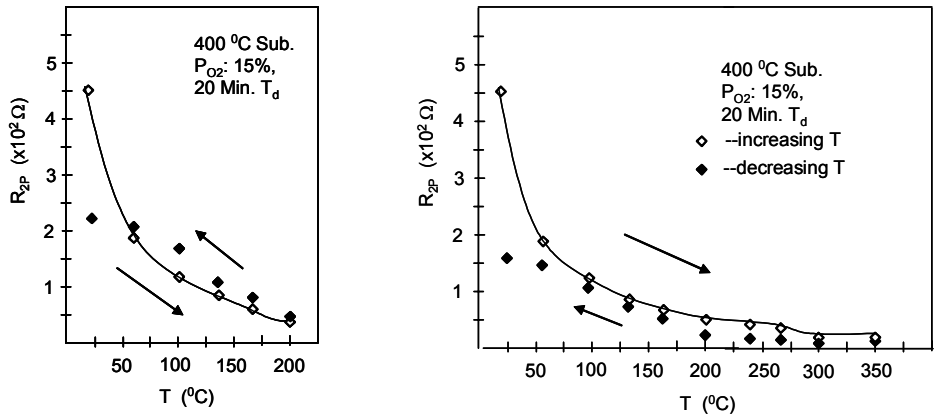


Fig. 8-6-2. Thermo-resistance curves of the films (sample V2) grown at 400 ^{0}C substrate temperature with 15% P_{O2} and different range of the temperature change respectively.

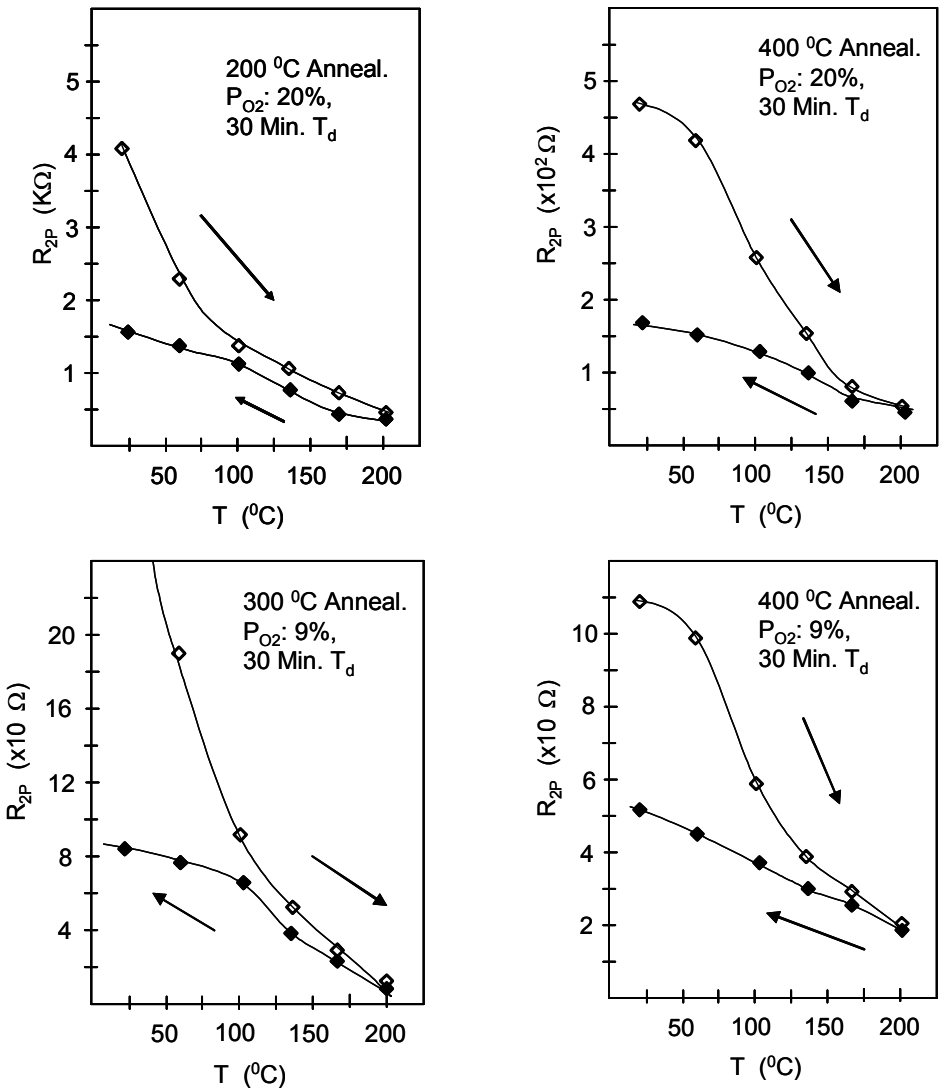


Fig. 8-6-3. Thermo-resistance curves of the 9% and 20% P_{O2} films (sample V4a, V3a, V6 and V1a) grown at room temperature, plus 200 ^{0}C, 300 ^{0}C and 400 ^{0}C post annealed respectively.

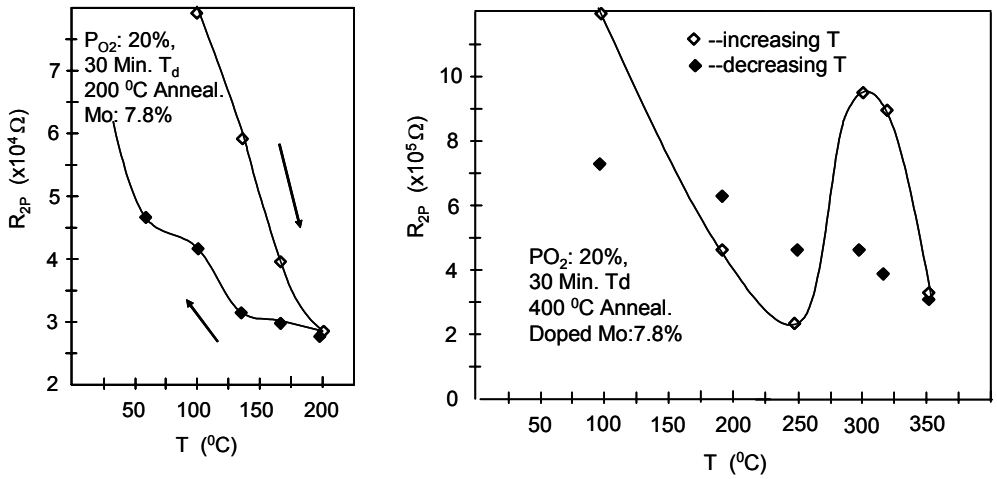


Fig. 8-6-4. Thermo-resistance curves of the 7.8% Mo doped films (sample VM2a2 and VM2a4) grown with 20% P_{O2} and annealed at 200 ^{0}C and 400 ^{0}C respectively.

Fig. 8-6-1 and Fig. 8-6-2 show the T- R_{2P} curves of the films (sample V8, V7, and V2) deposited at 200 ^{0}C and 400 ^{0}C T_s. There is no clear T- R_{2P} hysteresis behavior in the films deposited at 400 ^{0}C T_s. A small anti-hysteresis behavior was found, in the circle range of RT-200 ^{0}C for the films deposited at 400 ^{0}C T_s. They have a much wider bottom part in hysteresis curve for sample deposited at 200 ^{0}C and 15% P_{O2}. The maximum change of the R_{2p}/T rate can reach 260 Ω/^{0}C for the sample with 200 ^{0}C T_s (15% P_{O2}). The maximum change of the R_{2p}/T rate reaches 160 Ω/^{0}C for the sample with 200 ^{0}C T_s (9% P_{O2}).

The films (sample V4a, V3a, V6 and V1a), which were deposited at RT with different P_{O2} plus 200-400 ^{0}C post annealing treatment, have hysteresis in the T- R_{2P} curves after heating the samples in the circle temperature range (RT-200 ^{0}C) in Fig. 8-6-3. The maximum change of R_{2p}/T can reach 52 Ω/^{0}C for the sample with 20% P_{O2} (200 ^{0}C T_a). For the sample with 20% P_{O2} (400 ^{0}C T_a), the maximum change rate of R_{2p}/T can reach 40 Ω/^{0}C. In the sample of 9% P_{O2} (300 ^{0}C T_a), the maximum change of R_{2p}/T is 2.3 Ω/^{0}C. For the sample of 9% P_{O2} (400 ^{0}C T_a), the maximum change of R_{2p}/T reaches 0.8 Ω/^{0}C.

In Fig. 8-6-4 the 7.8% Mo doped V_2O_5 films (sample VM2a2 and VM2a4), which were deposited at RT and 30% P_{O2}, plus 200 ^{0}C and 400 ^{0}C post annealed, have a R_{2P} that change after heating in the temperature range RT-200^{0}C and RT-350 ^{0}C respectively. The R_{2P} of the films have an hysteresis. The 200 ^{0}C annealed sample has a much wider bottom part in the hysteresis curve, comparing with the pure V_2O_5 film in Fig. 8-6-3. The 7.8% Mo doped V_2O_5 film has much a higher R_{2P} value. The 400 ^{0}C annealed sample has a similar behavior, but its R_{2P} has a peak of 8.5 x 10^5 Ω at 300 ^{0}C. The color of all Mo doped V_2O_5 films changed from light yellow to grey yellow after the annealing. The other Mo doped (11.1%-18.9% ratio) V_2O_5 films show no variation of the resistance with temperature. For the sample with 400 ^{0}C T_a the maximum change of R_{2p}/T reaches 1200 Ω/^{0}C. The maximum change of R_{2p}/T reaches 560 Ω/^{0}C for the sample with 200 ^{0}C T_a.

In summary, the Mo doped V_2O_5 films show a much stronger TT behavior. Comparing all data of the pure V_2O_5 samples, the 20% P_{O2} and 7.8% Mo doped V_2O_5 film has a better TT property than the 9% P_{O2} and 15% P_{O2} films (maximum change of R_{2p}/T). It is deduced that the T- R_{2P} hysteresis behavior and anti-hysteresis behavior comes from the change of the films from a semiconductor to a metallic phase [4]. All

these properties of the films indicate that V_2O_5 films have a good thermotropic behavior and they are good TT materials.

8.7. XPS Spectra of the V_2O_5 Films

XPS measurements of the films and comparison with the standard spectra clearly indicated that the samples are mainly composed by V_2O_5. Fig. 8-7-1, Fig. 8-7-2, and Fig. 8-7-3 show the XPS spectra of the V_2O_5 films in the oxygen 1s, vanadium 2p and molybdenum 3d regions. The main oxygen peak 530.2 eV was found as expected for vanadium bonded oxygen. The shoulder at larger energy is due to oxygen bonded with the surface carbon. Cazzanelli *et al.* indicated that the oxygen shoulder peak disappears in the bulk material[38].

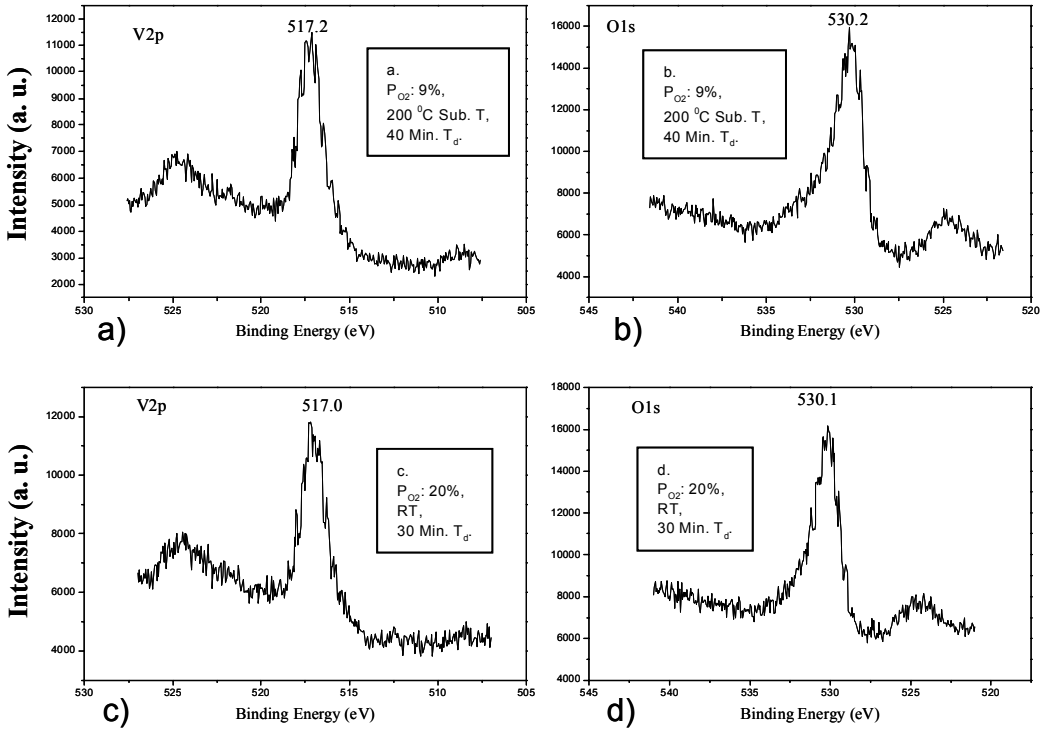


Fig. 8-7-1. XPS spectra of 9% P_{O2} V_2O_5 thin film deposited at 200 ^{0}C for 40 minutes (a, b) and XPS of 20% P_{O2} V_2O_5 film deposited at room temperature for 30 minutes(c, d).

In the Figures the two peaks of vanadium correspond to a doublet $V2p_{3/2}$ (~517.1 eV) and $V2p_{1/2}$ (~524.3 eV), in which one is for the 3/2 and the other is for the 1/2 spin-orbit split components. The appearance of a weak band near 522 eV is attributed to the X-ray satellite of the O(1s) core level. All these samples showed narrow $V2p_{3/2}$ peaks, centered between 517.0 and 517.2 eV, a value which is very close to the reported ones

for crystalline V_2O_5 (517.6 eV, Perkin-Elmer Atlas) and standard V_2O_5 powder (517.2 eV) [39].

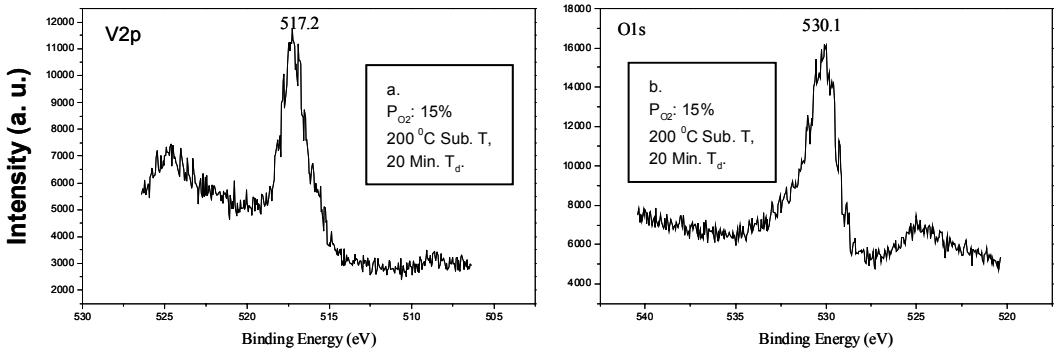


Fig. 8-7-2. XPS spectra of 15% P_{O2} V_2O_5 thin film deposited at 200 ^{0}C for 20 minutes.

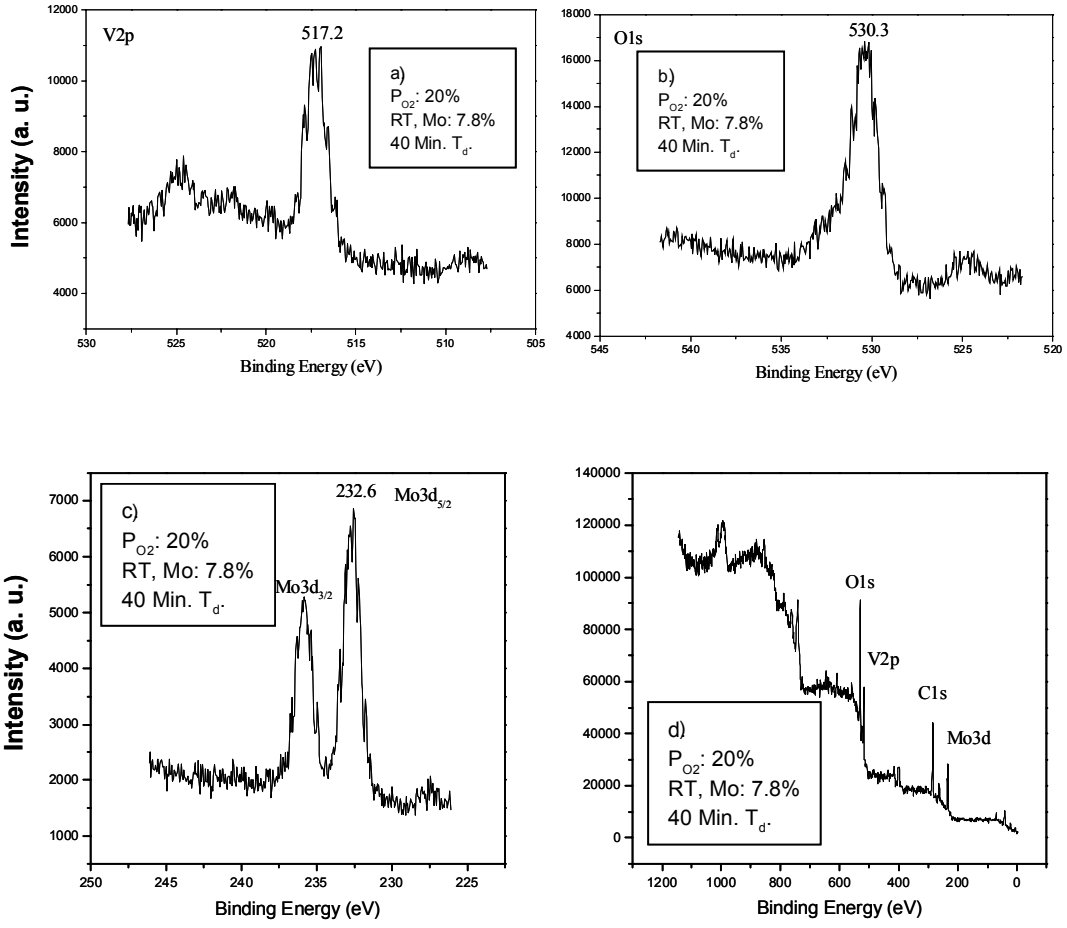


Fig. 8-7-3. XPS spectra of V_2O_5-MoO_3 thin film deposited with 7.8% Mo doping and 20% P_{O2} at room temperature for 40 minutes.

From the data of V_2O_5 powder, $V2p_{3/2}$ has a single peak at 517.2 eV with FWHM (full-width at half-maximum) of 1.6 eV. The $V2p_{3/2}$ of metal vanadium has a single peak at 512.2 eV [40]. The $V2p_{3/2}$ peaks of V_3O_5 and V_4O_7 are at 515.5 and 515.9 eV respectively[41]. The peaks of the samples deposited with lower P_{O2} are broader (Fig.8-7-1). The comparison with other reported XPS data, positions and spin-orbit split constants, is given for different vanadium oxides in Table 8-2-1. The comparison of the experimental data with those reported in the literature indicate that the oxide formed under these conditions is not V_2O_3, VO_2 and other vanadium oxides other than V_2O_5. This confirms that the grown films are composed by V_2O_5.

Table 8-2-1. Core levels binding energies and spin-orbit splitting constant δ′ between the levels $V2p_{3/2}$ and $V2p_{1/2}$.

Core level	Binding energies (eV)							
	Exp.	V_2O_5		VO_2		V_2O_3	
$V2p_{3/2}$	517.0 ~517.2	516.9	517.6	516.1	516.2	515.5	515.7
$V2p_{1/2}$	524.1~524.4	524.3	524.4	523.1	523.5	523.0	523.3
δ′	7.1~7.5	7.4	7.5	7.0	7.3	7.6	7.6
Ref.	-	[42]	[40]	[43]	[42]	[44]	[42]

The oxidation state of the Mo was also characterized using XPS. Fig. 8-7-3 shows the XPS spectrum of the V_2O_5-MoO_3 thin film deposited with 7.8% Mo doping and 20% P_{O2} for 40 minutes. Fig. 8-7-3 a) and b) display the XPS spectra of V (2p) and O(1s) core levels. The XPS spectrum of the MoO_3 film displays the characteristic doublet $Mo3d_{5/2}$ at 232.6 eV and $Mo3d_{3/2}$ at 235.8 eV in Fig. 8-7-3c. The doubling Mo (3d) line separated by 3.2 eV and their intensity ratio is 2:3. Since the $Mo3d_{5/2}$ binding energy of Mo, MoO_2 and MoO_3 is 228.0, 229.4 and 232.6 eV respectively [45], This indicates that the lines correspond to peaks of Mo^{6+} ions in MoO_3 with d^0 electron configuration [46].

8.8. XRD of Vanadium Oxide Films

In order to study the film structure, XRD spectra were measured on the samples. Fig. 8-8-1 shows the X-ray spectra of the vanadium oxide films with 15% P_{O2} and the effects of annealing and substrate temperature. In curve (D), only very weak peaks plus a broad background from the glass substrate can be observed, which indicates that the film obtained at RT is amorphous. The films prepared with 400 ^{0}C annealing have no sharp

peak too in their X-ray diffraction spectra. Only very weak peaks of V_2O_5 (400), VO_2 (B´) (002) and V_2O_5 (002) [30], plus a broad background from the glass substrate can be observed in the curve (C), because the films were amorphous and thin. The spectrum (B) shows the peak that coincides with the peak VO_2 (B´)(001), V_2O_5 (001), V_2O_5 (400), and V_2O_5 (002)[30, 47]. VO_2 (B´) is a metastable compound which can be converted into stable VO_2 with a rutile or monoclinic structure in some conditions. Its structure is derived from the orthorhombic V_2O_5 by a crystallographic shear belonging to the same series as V_6O_{13} [48]. VO_2 (B´) was reported by Sata *et al.* [47] to be an intermediate phase between V_2O_5 and V_2O_3. Although there are many possible phases of vanadium oxides, the X-ray analysis revealed that the 15% P_{O2} deposited films are VO_2 (B´) and V_2O_5. The IR analysis of the section 8.4 also confirms the XRD analysis. All the films were strongly oriented with respect to VO_2 (B') (001), V_2O_5 (001), and V_2O_5 (100). The structure correlates mainly with substrate temperature (T_s) and little with annealing temperature.

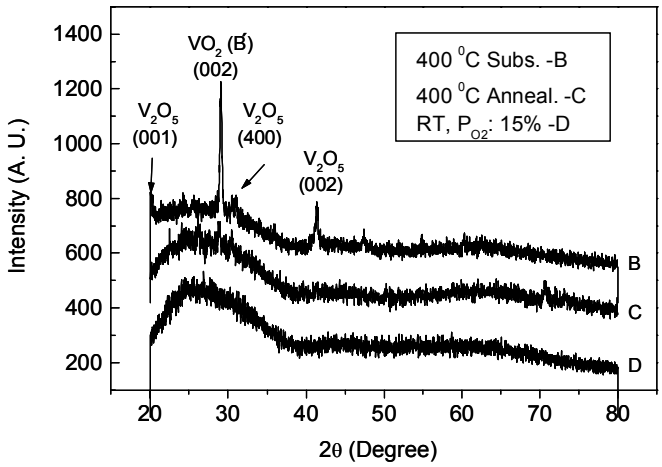


Fig. 8-8-1. X-ray diffraction spectra of vanadium oxide films deposited with 15% P_{O2} at 400 ^{0}C substrate temperature (B), after 400 ^{0}C annealing (C), and at room temperature deposition (D).

Fig. 8-8-2 shows the X-ray diffraction patterns for 18.9% Mo doped V_2O_5 films (30% P_{O2}) at RT and 400 ^{0}C annealing temperature, respectively. The XRD pattern of the sample C deposited at RT consists of a broad hump and not has well defined diffraction peak. After 400 ^{0}C annealing, the V_2O_5 (400) peak of sample B becames stronger than that of the sample C and of the pure V_2O_5 film annealed at 400 ^{0}C (Fig. 8-8-1 C). This indicates a slight modification in the V_2O_5 structure after MoO_3 mixing and post-annealing. Moreover, as shown in Fig. 8-8-2, the new peaks in the diffraction pattern

have emerged which are assigned to MoO_3 [28]. This is in agreement with the result of Patil *et al.* [49] .

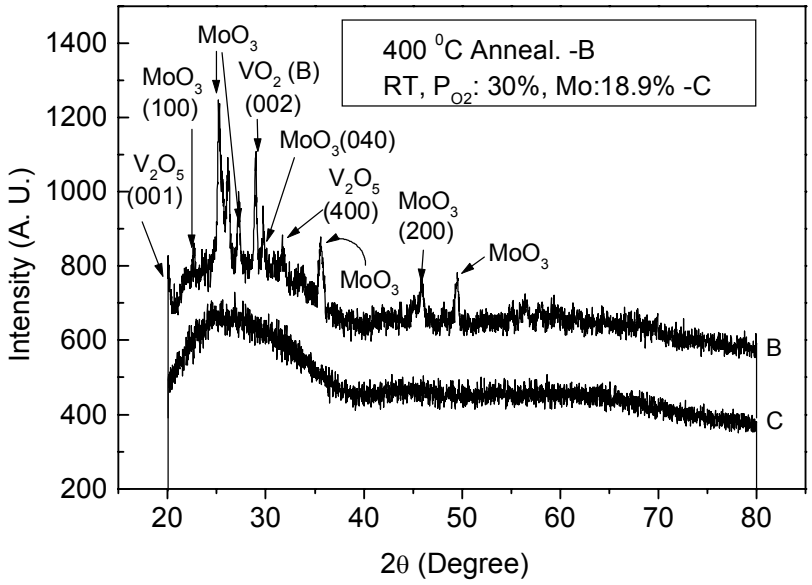


Fig. 8-8-2. X-ray diffraction patterns of V_2O_5 films, which were deposited in 18.9% Mo doping, 30% $P_{O2,}$ room temperature and 400 ^{0}C annealing.

8.9. Film Micrographs Using SEM, AFM and Surface Analysis Software

Fig. 8-9-1 and 8-9-2 are SEM micrographs of the surface and cross section of the V_2O_5 films. The V_2O_5 film, which was deposited with 9% P_{O2} at RT for 35 minutes, is shown in Fig. 8-9-1. The SEM cross section and surface views show that a dense and uniform film was observed. The SEM of the 19% Mo doped V_2O_5 film that was deposited with 30% P_{O2} at RT for 60 minutes, is shown in Fig. 8-9-2. Defects and a few big particles appear in the samples. The one or zero big particle per μm^2 is distributed randomly on the surface.

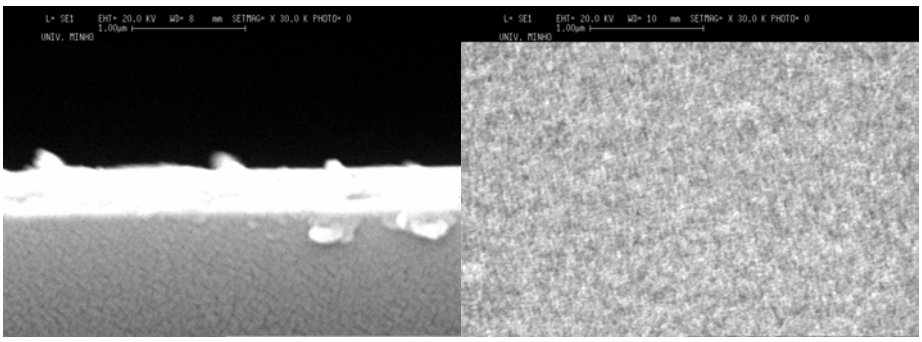


Fig. 8-9-1. Topography and SEM cross section of the V_2O_5 film deposited with 9% oxygen partial pressure at room temperature for 35 minutes.

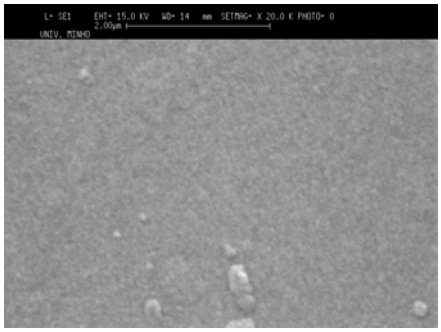


Fig. 8-9-2. Topography of 19% doped Mo V_2O_5 film deposited with 30% oxygen partial pressure at room temperature for 60 minutes.

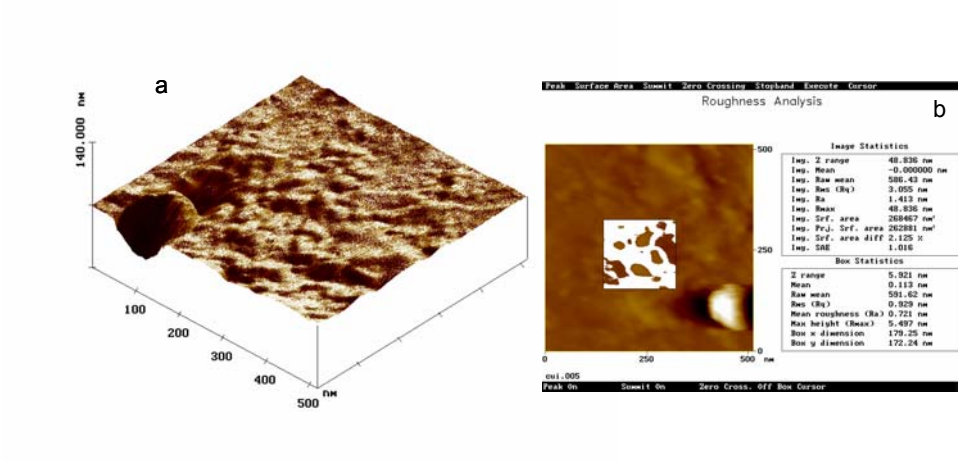


Fig. 8-9-3. Three dimensions (3D) AFM image (a) and roughness image (b) of V_2O_5 film deposited with 9% oxygen partial pressure at room temperature for 35 minutes.

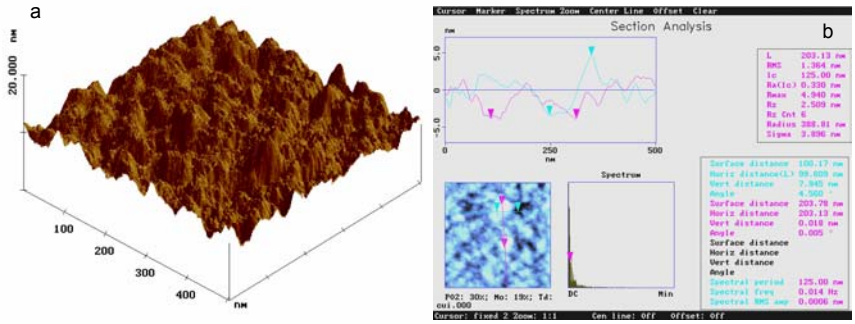


Fig. 8-9-4. Three dimension (3D) AFM image (a) and section analysis (b) of 19% Mo doped V_2O_5 film deposited with 30% oxygen partial pressure at room temperature.

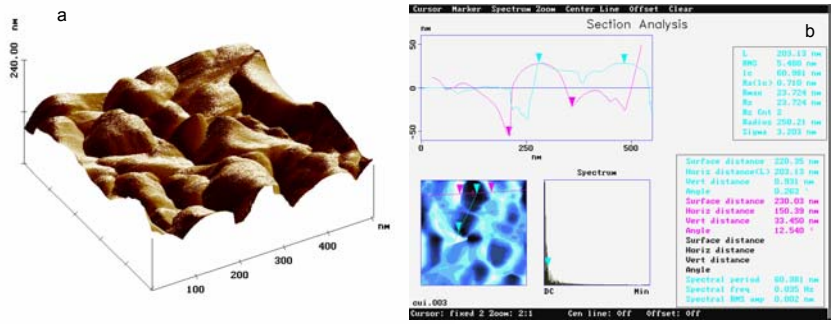


Fig. 8-9-5. AFM image (a) and section analysis (b) of the 19% Mo doped V_2O_5 film deposited with 30% oxygen partial pressure and annealed at 400 ^{0}C for 60 minutes.

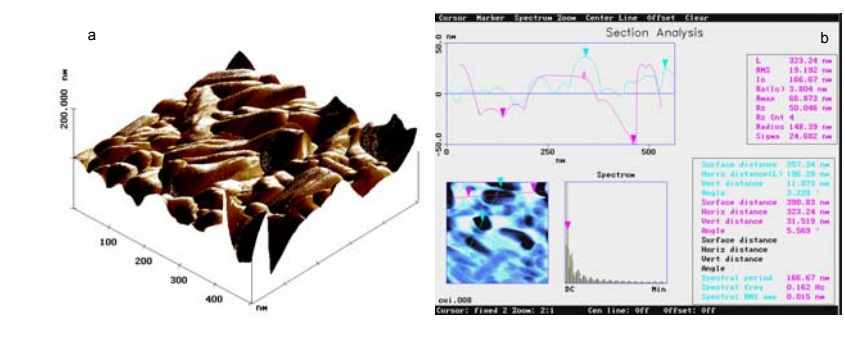


Fig. 8-9-6. AFM image (a) and section analysis (b) of V_2O_5 film deposited with 15% P_{O2} and at 400 ^{0}C substrate temperature (Ts) for 20 minutes.

The three dimensional (3D) AFM image (Fig. 8-9-3) of V_2O_5 film (9% P_{O2}) was taken in order to further observe microstructure and confirm the SEM result of Fig. 8-9-1. The finer morphology and roughness of the films can be clearly seen. We can conclude that the grain size is uniform. The photography and AFM software analysis reveals a uniform growth of the film. The average grain size is less than 60 nm. Fig.8-9-3 (b) presents a surface profile and the surface roughness data determined by AFM software analysis. The small box area of Fig. 8-9-3 (b) is in a real size and scale comparing with the whole zone of 500×500 nm, but it was treated in different background and contrast. The maximum roughness is 5.5 nm in the small box area and 48.8 nm in the whole zone of 500×500 nm.

In order to further observe the microstructure and confirm the SEM result of Fig. 8-9-2, the 3D AFM image of the 19% Mo doped V_2O_5 film, which was deposited with 30% P_{O2} at RT for 60 minutes, is shown in Fig. 8-9-4 (a). The morphology and roughness of the films is clearly seen. The average grain size is about 70 nm. In Fig. 8-9-4 (b) a section analysis, and data determined by AFM software analysis was presented. The maximum roughness and average RMS roughness is 4.9 and 1.4 nm, respectively.

Fig. 8-9-5 (a) shows the AFM image of 19% Mo doped V_2O_5 film deposited with 30% P_{O2} for 60 minutes and annealed at 400 ^{0}C. It is seen that there are much bigger grains formed in the film, also it has a good uniformity revealing a uniform growth of the films. The average grain size is about 130 nm. In Fig. 8-9-5 (b) it is presented a section analysis of the film and data determined by AFM software analysis. The maximum roughness and average RMS roughness are 23.7 and 5.5 nm, respectively. The results showed an increase in the roughness after thermal treatments. Also the film in Fig. 8-9-5 shows higher roughness than the sample in Fig.8-9-4.

Fig. 8-9-6 (a) shows the AFM image of the V_2O_5 film deposited with 15% P_{O2} at 400 ^{0}C substrate temperature (T_s) for 20 minutes. It is clearly seen that there are much bigger quasi bar-shape grain formed in the film. Also it has a good uniformity revealing a uniform growth of the films. The average grain dimensions are less than 55×135 nm. Fig. 8-9-6 (b) presents a section analysis and data determined by the AFM analysis. The maximum roughness and the average RMS roughness are 66.9 and 19.2 nm. Comparing Fig. 8-9-5 and Fig. 8-9-6, the grain size of the V_2O_5 film deposited with 15% P_{O2} at 400 ^{0}C T_s is much bigger than that of the film annealed at 400 ^{0}C. By the theory analysis [48] the bar-shaped grains may come from combining the effect of the direction of flowing field of the sputtering gas and the thermal field of high 400 ^{0}C T_s (Section 6.8.7).

After thermal treatments, the increase of roughness can be explained by the grain growth, sintering process and some structure densification of the coatings [51, 52]. The decrease of the maximum roughness of the V_2O_5 sample with decreasing P_{O2} (for example, Fig. 8-9-3 and box area of Fig. 8-9-4) can be explained by the growing rate of the films. The randomly distributed big grains in the films can be explained by the polycrystalline nature of vanadium with some re-nucleation of molybdenum or vanadium crystals during the deposition process [53, 54].

8.10. Summary of the Chapter

In this chapter we reported the characteristics of vanadium oxide (V_2O_5) and V_2O_5 – MoO_3 thin films using UV-vis-NIR, IR, XRD, XPS, SEM and AFM methods. The samples were deposited by dc reactive sputtering using a vanadium target in different conditions.

In the UV-Vis NIR studies it was found that as the T_s (substrate temperature) increases from RT to 400 ^{0}C, the transmittance of the films in the 300 nm ~ 3200 nm region decreases, the thickness increases and the color of the film changes from light yellow to yellow at the higher T_s. As the Mo doping ratio increases from 0 to 18.9%, the transmittance of the films decreases. The absorption edge (~450 nm) of transmittance of the films shifts to lower wavelengths as the Mo doping ratio increases.

The IR vibration results of the as-deposited V_2O_5 films were compared to that of the annealed films. Detailed IR modes assignments of the films measured by IR reflection-absorbance in NGIA (near grazing incidence angle) were given. It is clearly seen that as the annealing temperature increases from RT to 400 ^{0}C, the peak at 970 cm^{-1}, shoulder peak at 1020 cm^{-1} and peak at ~1200 cm^{-1} of the films increase and the peaks at 517 and 418 cm^{-1} decrease. The effect of P_{O2} during the deposition of the V_2O_5 films grown at 200 ^{0}C substrate temperature (T_s) in 15% P_{O2} and 20% P_{O2}, was discussed. It is seen that the absorbent peak at 970 and 1020 cm^{-1} become stronger after depositing at 200 ^{0}C T_s. The shift of the strong band between 1140 cm^{-1} and 1220 cm^{-1}, which is assigned to δ(w-o) in the M-OH…H_2O group, was observed as the plane deformational (bending) M-O mode. This shows that the deposited films are V_2O_5 and VO_2, because the VO_2 shoulder peaks at 508 cm^{-1} and 714 cm^{-1} do appear in the IR spectra. There is a clear increase of the 535 cm^{-1} peak of MoO_3 as the Mo doping ratio is increased. These results were confirmed by the XPS study. The IR spectra of V_2O_5 –MoO_3 films (Mo doping ratio less than 20%) shows broad bands poorly resolved and are found to be more or less similar to that of V_2O_5 in our experiments. This indicates that the structure of V_2O_5 is not deeply modified upon the incorporation of small quantities of MoO_3.

These films were investigated for thermochromic and thermo-resistance applications. The films exhibit clear changes in transmittance when the temperature is varied, specially in the 3600-4000 cm^{-1} range. After applying higher T (>T_c) to the samples, the as-RT deposited films with 9% P_{O2} has a transmittance variation of 30%, but the films that were deposited on a heated substrate of 400 ^{0}C have little variation. The maximum

variation of transmittance of the Mo doping sample reaches 49% at 4000 cm^{-1}. There is tendency of bigger variation of transmittance when the Mo doping ratio of the film or the P_{O2} of the film is larger, after applying temperature of 200 ^{0}C to the samples.

The films exhibit changes in resistance in the RT-350 ^{0}C range except the ones which were grown at RT. The maximum change of R_{2p}/T can reach 1200 Ω/^{0}C. It is seen that the Mo doped V_2O_5 films show much stronger TT properties. The films which were grown at RT show no resistance variation if the increasing temperature is less than 100 ^{0}C. All these properties of the films indicate that V_2O_5 films have good thermochromic and thermotropic behavior in the 3600-4000 cm^{-1} range and thermotropic behaviors. They are good TC and TT materials.

The XPS peaks of the sample deposited with lower P_{O2} are broader. XPS measurements on the surface clearly indicate that the samples are mainly composed of V_2O_5. All the samples showed narrow $V2p_{3/2}$ peaks (FWHM: ~1.6 eV), centered between 517.0 and 517.2 eV, a value which is very close to the reported ones for crystalline V_2O_5 (517.6 eV) and standard powder of V_2O_5 (517.2 eV). The pair of vanadium peaks corresponds to a doublet $V2p_{3/2}$ (517.1 eV) and $V2p_{1/2}$ (524.3 eV), in which one is for the 3/2 and the other is for the 1/2 spin-orbit split components. The XPS spectra of the MoO_3 films display the characteristic doublet $Mo3d_{5/2}$ at 232.6 eV and $Mo3d_{3/2}$ at 235.8 eV.

XRD of the sample revealed structural information of the film. An amorphous film was obtained at RT. Only very weak peaks of V_2O_5 and MoO_3 plus a broad background from the glass substrate could be observed. The films prepared with 400 ^{0}C annealing have no sharp peaks too in their X-ray diffraction spectra. The spectrum of the deposited films with 400 ^{0}C T_s shows peaks that coincided with VO_2 (B′) (001), V_2O_5 (001), V_2O_5 (400), and V_2O_5 (002).

SEM and three dimensional (3D) AFM images of the V_2O_5 films were taken in order to further observe the microstructure. The finer morphology and roughness of the films was clearly seen. We concluded that the grain size is uniform. The average grain size ranges from 60 nm to 135 nm.

From the above results, it can be concluded that dc sputtered vanadium oxide films non doped or doped the desired amount of Mo are potential candidates for advanced thermochromic, thermo-resistance and electrochromic devices.

8.11. References

[1] J. P. Pereira-Ramos, R. Messina, J. Perichon, J. Appl. Electrochem 16 (1986) 379.

[2] H. K. Park, W. H. Smyrl, M. D. Ward, J. Electrochem. Soc. 142 (1995)15.

[3] K. Wiesener, W. Schneider, D. Ilic, E. Steger, K. H. Hallmeier, E. Brackmann, J. Power Sources 20 (1987) 157.

[4] P. Jin, S. Tanemura, "$V_{1-x}Mo_xO_2$ thermochromic films deposited by reactive magnetron sputtering", Thin Solid Films 281-282(1996)239-242.

[5] S. Saitzek, G. Guirleo, F. Guinneton, L. Sauques, S. Villain, K. Aguir, Ch. Leroux, J. R. Gavarri, New thermochromic VO2-CeO2 bilayers for optical or electronic switching systems. - Thin Solid films, 449, 1-2, 166-172, 2004

[6] F. Guinneton, J. C. Valmalette, J. R. Gavarri, Nanocrystalline vanadium dioxide: synthesis and mid-infrared properties, Optical Materials, 15(2)(2000) 111-114.

[7] C. G. Granqvist, Handbook of Inorganic Electrochromic Materials, Elsevier, Amsterdam, 1995.

[8] S. F. Cogan, N. M. Nguyen, S. J. Perrotti, R. D. Rauh, J. Appl. Phys. 66 (1989) 1333.

[9] R. Angelucci,A. Poggi,L. Dori, G.C. Cardinali,A. Parisini,G. Pizzochero, F. Trinro, F. Cavani,C. Critelli,L. Boarino,Thin Solid Films 297 (1997) 43.

[10] A. Lavacchi, B. Cortigiani, G. Rovida, U. Bardi, A. Atrei, R. Angelucci, L. Dori, S. Nicoletti, A. Poggi, Sensor Actuator B 71 (2000) 123.

[11] A. Z. Moshfegh, A. Ignatiev, Thin Solid Films 198 (1991) 251.

[12] M. Benmoussa, E. Ibnouselghazi, A. Bennouna, E. L. Ameziane, Thin Solid Films 265 (1995) 22.

[13] E. Kusano, J. A. Thell, J. A. Thornton, J. Vac. Sci. Technol. A6 (1988) 1663.

[14] A. Davies, R. J. Hobson, M. J. Hudson, W. J. Macklin, R. J. Neat, J. Mater. Chem. 6 (1996) 49.

[15] A. Surca, S. Bencic, B. Orel, B. Philar, Electrochim. Acta 44 (1999) 3075.

[16] Y. M. Li, T. Kudo, Solid State Ionics. 186-88 (1996) 1295.

[17] Y. M. Li, T. Kudo, Sol. Ener. Mater. & Sol. Cells 39 (1995) 179.

[18] D. Keomani, J.-P. Petit, D. Deroo, Sol. Ener. Mater. & Sol. Cells 36 (1995) 397.

[19] M. Di. Gulio, D. Manno, G. Micocci, A. Serra, A. Tepore, Phys. Stat. Sol. A168 (1998) 249.

[20] R. H. Jarman, A. K. Cheetam, Mat. Res. Bull. 17 (1982) 1011.

[21] K. Narushima, I. Shiozaki, Solid State Commun. 101 (1997) 99.

[22] M. A. Quevedo-Lopez, R. Ramirez-Bon, R. A. Orozco-Teran, O. Mendoza-Gonzalez, O. Zelaya-Angel, " Effect of a CdS interlayer in thermochromism and photochromism of MoO_3 thin films", Thin Solid Films 343-344 (1999) 202-205.

[23] S. M. Babulanam, T. S. Eriksson, G. A.Niklasson and C. G. Granqvist, , Sol. Energy Mater., 16 (1987) 347.

[24] P. Jin and S. Taemura, Jpn. J. Appl. Phys., 34 (1995) 2459.

[25] C. G. Granqvist, Materials Science for Solar Energy conversion Systems, Pergamon, Oxford, 1991.

[26] R. Eujalbert, J. Galy, Acta Cryst. C. 42 (1986) 1467-1469.

[27] W. Lambrecht, B. Sjafari-Rouhani , J. Vennik, J. Phys. C: Solid State Phys., 19 (1986) 369.

[28] E. I. Altman, T. Droubay, S. A. Chambers, " Growth of MoO3 films by oxygen plasma assisted molecular beam epitaxy", Thin Solid Films 414 (2002) 205-215.

[29] V. V. Fomichev, P.I. Ukrainskaya, T. M. Ilyin, "Vibrational spectra and electrostatic fields of V_2O_5 and lithium vanadium bronzes", Spectrochimica Acta part A 53 (1997) 1833-1837.

[30] A. Surca, B. Orel, Electrochimica Acta 44 (1999) 3051-3057.

[31] G. A. Nazri, C. Julien, Solid State Ionics 53-56 (1992) 376.

[32] P. Clauws, J. Broeckx, J. Vennik, Phys. Status solidi (b) 131 (1985) 459.

[33] K. V. Madhuri, B. S. Naidu, O. M. Hussain, M. Eddrief, C. Julien, "Physical investigations on electron beam evaporated V_2O_5-MoO_3 thin films", Materials Sci. and Engineering B86 (2001) 165-171.

[34] B. Bootz, H. Finkenrath, G. Franz, N. Uhle, Solid State Comm. 13 (1973) 1477.

[35] I. L. Botto, M. B. Vassallo, E. J. Baran, G. Minelli, "IR spectra of VO_2 and V_2O_3", Materials Chemistry and Physics 50 (1997) 267-270.

[36] D. Adler, "Thermochromic Compounds" Rev. Mod.Phys.40 (1968) 714.

[37] N. F. Mott, Metal Insulator Transitions, Taylor and Francis, Ltd. London, UK (1974).

[38] E. Cazzanelli, G. Mariotto, S. Passerini, W. H. Smyrl, A. G Orenstein, "Raman and XPS characterization of vanadium oxide thin films deposited by reactive RF sputtering", Solar energy Materials & Solar Cells 56 (1999) 249-258.

[39] M. Ghanashyam Krishna, Y. Debauge, A. K. Bhattacharya, "X-ray photoelectron spectroscopy and spectral transmittance study of stoichiometry in sputtered vanadium oxide films", Thin Solid Films, 312 (1998) 116-122.

[40] J. Chastain (Ed), Handbook of X-ray Photelectron Spectroscopy, Perkin-Elmer, Eden Praire, MN, 1992.

[41] M. Demeter, M. Neumann, W. Reichelt, Surf. Sci. 454-456 (2000) 41.

[42] G. A. Sawatzky, D. Post, Phys. Rev. B 20 (1979) 1546.

[43] J. Kasperkiewicz, J. A. Kovacich, D. Lichtman, J. Electron Spectrosc. Rel. Phen. 32 (1983) 123-132.

[44] R. J. Colton, A. M. Guzman, J. W. Rabalais, J. Appl. Phys. 49 (1978) 409.

[45] T. H. Fleisch, G. J. Mains, J. Chem. Phys. 76 (1982) 780.

[46] R. B. Firment, A. Ferretti, Surf. Sci. 129 (1983) 155.

[47] X. J. Wang, H. D. Li, Y.J. Fei, X. Wang, Y. Y. Xiong, Y. X. Nie, K. A. Feng, "XRD and Raman study of vanadium oxide thin films deposited on fused silica substrates by RF magnetron sputtering", Appl. Surf. Sci., 177 (2001) 8-14.

[48] R. M. German, Powder Metallurgy Science, Metal Powder Industries Federation, Princeton, NJ (1984)

[49] F. Theohald, R. Cabala, J. Bernard, J. Solid State Chem. 17 (1976) 431.

[50] P. R. Patil, P. S. Patil, "Preparation of mixed oxide MoO_3-WO_3 thin films by spray pyrolysis technique and their characterisation", Thin Solid Films 382 (2001) 13-22.

[51] Nicolas Martin, Christophe Rousselot, Daniel Rondot, FrancK Palmino,René Mercier, Thin Solid Films, 300 (1997) 113-121.

[52] Takahashi T, NaKabayashi H , Terasawa T, Masugata K. J. Vac. Sci. Technol., A20(4) (2002) 1205-1209.

[53] Schofield MA, Aita CR, Rice PM and Gajdardziska-Josifovska M. Thin Solid Films, 326 (1998) 106-116.

[54] Schofield MA, Aita CR, Rice PM and Gajdardziska-Josifovska M. Thin Solid Films, 326 (1998) 117-125.